Available online at www.sciencedirect.com
ScienceDirect
Acta Materialia 56 (2008) 4601–4607
Acta MATERIALIA
www.elsevier.com/locate/actamat

Experimental and theoretical study of lattice relaxation around refractory atoms in nickel

V. Koteski [a,c,*], H.-E. Mahnke [a,b], J. Belošević-Čavor [c], B. Cekić [c], G. Schumacher [a]

[a] Hahn-Meitner-Institut Berlin GmbH, Bereich SF, Glienicker Strasse 100, D-14109 Berlin, Germany
[b] Freie Universität Berlin, Fachbereich Physik, Arnimallee 14, D-14195 Berlin, Germany
[c] Institute of Nuclear Sciences Vinca, P.O. Box 522, 11001 Belgrade, Serbia

Received 26 February 2008; received in revised form 8 May 2008; accepted 13 May 2008
Available online 19 June 2008

Abstract

The lattice relaxation around Mo, Ru, Hf, Ta, W and Re in Ni is investigated by means of X-ray absorption spectroscopy. For all of the investigated concentrations the substitutional lattice position is confirmed except for the higher Hf concentration where different phases are observed. An outward relaxation of the neighboring atoms is detected with clear trends of increasing nearest neighbor distances with decreasing valence for the 5d impurities, and separate trends for the 4d impurities. Ab initio supercell calculations within the linearized augmented plane wave formalism are used to complement the experimental results and allow for a better interpretation of the experimental trends in terms of the electronic structure of the impurity.

Keywords: Extended X-ray absorption fine structure (EXAFS, XANES); Nickel alloys; Augmented plane wave method (FLAPW)

1. Introduction

While in many important applications of metals and intermetallic phases the properties of materials can be tailored by introducing suitable alloying elements, the local structure and possible lattice relaxation around these elements is in general not very well known. Nickel-base superalloys are of significant technological importance, due to their very high strength (shear resistance and flow stress) at high temperatures, as compared to usual alloys such as steels. The last generations of superalloys include refractory elements, e.g. Mo, W, Ru, or Re, that help enhance their superior mechanical properties and corrosion resistance [1]. The strengthening effect is not fully understood in terms of the underlying mechanism, and efforts have been made to correlate it to structural, electronic or bonding features of the impurity system [2–4].

Ni-base superalloys consist of a face-centred cubic (fcc) Ni solid solution matrix (γ phase) in which the strengthening γ' phase (Ni_3Al-type) is dispersed. The lattice mismatch between the two phases is found to be an important parameter in controlling the properties of the superalloys [5–7]. It appears that one way of altering the lattice mismatch is by doping with refractory elements, which incorporated either into the γ or γ' phase, or into both, can contribute to the overall contraction or expansion of the corresponding lattice. The clustering of the refractory elements has also been attributed as one of the possible mechanisms of solid solution strengthening [2].

In the following we present the results of a combined, experimental and theoretical determination of the local structure around Mo, Ru, Hf, Ta, W and Re in nickel. In some model γ phases of Ni-base superalloys the addition of small amounts of Re, Mo, Ru and W were shown to affect short-range order (SRO) which is reflected by peaks of the {11/20} type. The SRO is approximately stable up to 600 °C and then decreases gradually up to about 1000 °C where it finally vanishes [8,9]. To date, the lattice

* Corresponding author. Address: Institute of Nuclear Sciences Vinca, P.O. Box 522, 11001 Belgrade, Serbia.
E-mail address: vkotes@vin.bg.ac.yu (V. Koteski).

1359-6454/$34.00 © 2008 Acta Materialia Inc. Published by Elsevier Ltd. All rights reserved.
doi:10.1016/j.actamat.2008.05.015

relaxation of these elements is not known with greater accuracy in either the γ or γ' phase. With additional input on the Ni_3Al, the presented results could be of special importance for modelling newer generations of alloys with superior properties.

In our work, X-ray absorption spectroscopy (XAS) is used as a tool to probe the local geometry around the refractory elements in Ni. Specifically, the extended X-ray absorption fine structure (EXAFS) is used to determine the local bond lengths, and lattice relaxation. In addition, the experimentally extracted information on the lattice relaxation around the investigated alloying elements is complemented with ab initio calculations within the framework of density functional theory (DFT).

2. Experimental and data analysis

Our samples were prepared from high-purity materials in a RF oven under Ar overpressure, after the oven chamber had been cycled several times from 10^{-5} mbar to Ar overpressure to reduce the oxygen partial pressure to below 10^{-14} ppm. To achieve a homogeneous distribution of impurities, the samples were turned over and remelted several times. After melting, the samples were quenched to room temperature. For selected cases where the possibility of cluster formation was anticipated, the samples were kept at around 700 °C for 30 min and afterwards they were allowed to cool down to room temperature over 27 h. Finally, the samples were cut and polished into slabs of approximately 10 mm×10 mm size and 0.5 mm thickness. For Ni:Hf, Ni:Ru and Ni:Re we prepared samples with several different concentrations, in the range 0.2–5 at.% of the added elements. This is found to be especially important in the case of Ni:Hf, where the solubility of Hf in the Ni matrix is relatively low. For Ni:Mo and Ni:W we used samples with 5 at.% of the added elements, whereas for Ni:Ta the Ta concentration was 2 at.%.

The local structure around the impurity atoms was investigated by EXAFS spectroscopy at the X1 beamline of HASYLAB at DESY. The measurements were performed in fluorescence mode using a seven-segment Ge detector. Using a liquid helium cryostat, the temperature for the set of investigated samples was kept between 20 and 140 K. Owing to the reduced "dynamical damping" of the EXAFS signal, the low-temperature measurements are important for obtaining good quality spectra. We collected fluorescence spectra at the K-edges of Mo, Ru, Hf, Ta and Re, and L_{III}-edges of W and Re.

The EXAFS spectra $\chi(k)$ were obtained after background subtraction using the ATHENA code [10]. The obtained $\chi(k)$ functions were subsequently multiplied by k and Fourier-transformed into R-space where the fitting procedure was performed. For the fitting we used ab initio theoretical standards computed with the FEFF8.2 code [11]. The fitting itself was performed using the ARTEMIS software package [10]. As an input to our FEFF calculations a cluster of 78 Ni atoms at ideal fcc positions was constructed, wherein the central Ni atom was replaced with the corresponding impurity atom. We employed the self-consistent field (SCF) [11] options provided within FEFF, therefore effectively enabling ab initio calculation of the Fermi energy and charge transfer between the atoms in the cluster. This, in principle, should enable a better theoretical description of the region with smaller k wavenumbers. In all investigated cases, except for Ni doped with 0.5% Re, where the statistics of the data was found to be insufficient to include higher shells, we have fitted the first four single scattering (SS) paths. In connection with the mean-square variations, σ^2, of each scattering path, the attempt to fit them jointly by using a single Debye temperature, θ_D, was unsuccessful, leaving us with the obvious choice of independently fitted σ^2s. In both the K and L_{III}-edge FEFF calculations an additional substantial contribution to the EXAFS signal was found to originate from three multiple scattering (MS) collinear paths possessing higher degeneracies, their major contributions in R-space appear around the fourth atomic shell. These paths were also included in the fitting of the data, but their structural parameters were expressed as a combination of the parameters of the corresponding SS paths wherever possible, therefore minimizing the set of variables. Their use in the fitting is not of crucial importance, but it contributes to the quality of the fits in the area around 5 Å. All the fits presented in this paper were performed using a Kaiser–Bessel window with a sill width of 1 $Å^{-1}$.

3. Details of calculations

Our calculations were performed using the WIEN97 (WIEN2k) implementations of the (linearized) augmented plane wave (LAPW) formalism [12,13]. In this formalism, the crystal space is divided into non-overlapping muffin-tin (MT) spheres around each atom, and in between regions. In the former the wave functions are expanded into atomic-like radial functions times spherical harmonics, while in the latter the basis set consists of plane waves. In our calculations we used a cut-off of l_{max}=10 for the waves inside the MT spheres, and $k_{max} = 8/R_{MT}^{min}$ for the plane waves, where R_{MT}^{min} is the smallest of the MT radii. The chosen values of $R_{MT} = 2.3$ a.u. for Hf, Ta, W and Re, $R_{MT} = 2.2$ a.u. for Mo and Ru, and $R_{MT} = 2.15$ a.u. for Ni were small enough to prevent any overlap of spheres when relaxation is included. The exchange and correlation effects were treated by using the most advanced generalized gradient approximation (GGA) [14]. The energy of −6 Ry was chosen to discriminate between the core and valence states. The calculations were spin-polarized and fully relativistic for the core states, whereas the scalar-relativistic approximation was used for the valence states.

In order to be able to treat our impurity systems with the WIEN code, due to the requirement of periodicity, a supercell had to be constructed. After the relaxation of the Ni fcc lattice, which gave 3.523 Å as a theoretical lattice constant, we constructed a $3 \times 3 \times 3$ supercell in fcc geometry (27

atom supercell). The obtained configuration effectively corresponds to a periodic array of impurities with a concentration of ~3.7% and an impurity–impurity distance of 7.47 Å. This enabled relaxation of two Ni atomic shells around the impurity, whereas the third Ni shell was fixed by the demands of symmetry. In the cases of Hf and Ta, in order to better describe the impurity systems, we also performed calculations with the $3 \times 3 \times 3$ in simple cubic symmetry (108 atom supercell), with an increased impurity–impurity distance of 10.6 Å and a decreased concentration of ~0.9%.

For the Brillouin zone (BZ) integration we used the tetrahedron method with 10 non-equivalent k-points in the irreducible wedge of the BZ. Given the size of the supercell, we found that our calculations sufficiently converged with respect to the selected k-points mesh. We also checked the convergence with respect to the other parameters of our calculations, especially examining the behaviour of the Hellmann–Feynman forces. As a criterion for force convergence the value of 1 mRy/a.u. was adopted.

4. Experimental results

4.1. Clustering effects

The possible clustering effect, tested by the annealing procedure described above, was investigated in the case of Mo and W. Fig. 1 depicts the measured absorption at the Mo K-edge in the annealed and non-annealed samples. As can be seen, there is no apparent difference in the measured absorption, which was found also to be the case after background removal and transformation into k-space of the corresponding EXAFS spectra. The same conclusion holds for the annealed and non-annealed W-doped samples. This means that our annealing treatment failed to produce clusters, at least to the extent that is detectable by EXAFS. This is no surprise, since the solubility of Mo and W is well above the investigated 5 at.%. On the other hand, investigations of model γ phases of several Ni-base superalloys by elastic diffuse neutron scattering as a function of temperature revealed pronounced SRO up to 600 °C [8,9]. Above this temperature SRO starts to decrease up to 1000 °C, where it vanishes completely. In one of these alloys revealing SRO, the sum of W and Mo element concentration is about 4 at.%. Hence, the solubility of W and Mo in real or model superalloys might be appreciably smaller compared to Ni resulting in SRO of DO22-type structure.

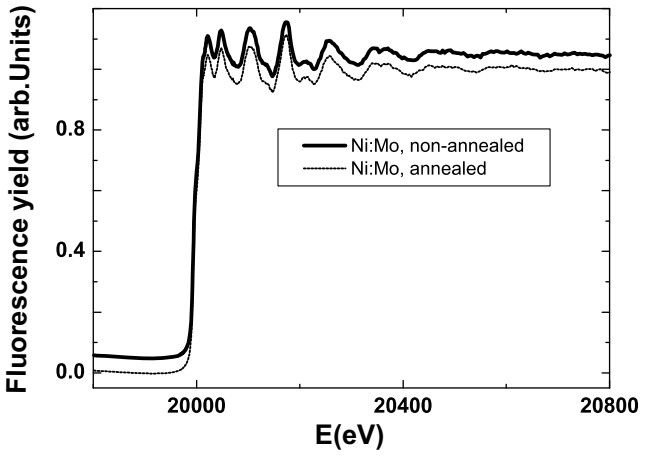

Fig. 1. Fluorescence yield spectra of Mo-doped Ni, measured around the Mo K absorption edge. Thick solid line: as prepared; thin dotted line: after annealing (see text).

4.2. 4d elements Mo and Ru in Ni

The k-weighted EXAFS spectrum of Mo-doped Ni collected at the Mo K absorption edge, along with its Fourier-transform is presented in Fig. 2. The coordination numbers of all the paths in our fit were fixed to their corresponding values in the pure compound, thus assuming substitutional local environment. A relatively good agreement between the experimental data and our model was obtained, which is also reflected in the value of the $\mathscr{R}$-factor of 0.8%. $\mathscr{R}$-factor (the goodness of fit) measures the deviation between theory and experimental data [15]. The values of the complete set of fitted parameters are given in Table 1, alongside with the parameters obtained by fitting the Ru-doped samples. Our result of 2.520(6) Å is in good agreement with the previous experimental result of 2.51 Å [16] obtained for 2 at.% of Mo in Ni by fitting with experimental standards.

In the case of Ru, samples with 0.2, 2 and 5 at.% of Ru in Ni were prepared. The Ni:Ru Fourier-transformed k-weighted EXAFS spectra at the Ru K-absorption edge are given in Fig. 3. Apart from the fair agreement between theory and data in all three cases ($\mathscr{R}$-factors from 1.4% to 1.6%) and relative similarity of the spectra, there are several differences. As can be seen from Table 1, a slight increase in the nearest neighbor (NN) Ru–Ni distance with concentration is observed. While this shift is still within the error bars, it is likely that it might be influenced by the short-range structural disorder. The structural disorder most likely is the cause of the decrease of the first shell peak amplitude, i.e. correspondingly of the increase of the Debye–Waller factors of the NN path as a function of Ru concentration.

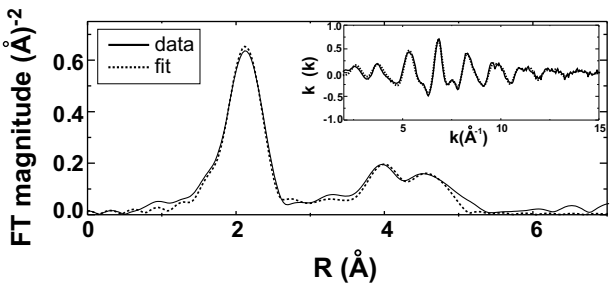

Fig. 2. Fourier-transform of the EXAFS oscillations of the Ni:Mo sample (solid line) and fit (dotted line). The corresponding EXAFS spectra are given in the inset.

Table 1
Fitted values from EXAFS data for the energy shift E_0, Debye–Waller factors σ, interatomic distances R, fit ranges ΔR and Δk, and S_0^2 for the first four coordination shells around Mo and Ru in Ni

	R_1 (Å)	R_2 (Å)	R_3 (Å)	R_4 (Å)
$Ni_{95}Mo_5$	2.520(6)	3.51(2)	4.37(1)	5.1(2)
$Ni_{99.8}Ru_{0.2}$	2.505(5)	3.51(2)	4.34(1)	5.0(1)
$Ni_{98}Ru_2$	2.506(4)	3.51(2)	4.34(1)	5.0(1)
$Ni_{95}Ru_5$	2.510(4)	3.52(2)	4.349(9)	5.1(1)
	σ_1 (Å^{-2})	σ_2 (Å^{-2})	σ_3 (Å^{-2})	σ_4 (Å^{-2})
$Ni_{95}Mo_5$	0.0045(7)	0.009(3)	0.008(1)	0.006*
$Ni_{99.8}Ru_{0.2}$	0.0022(2)	0.003(2)	0.0036(9)	0.003*
$Ni_{98}Ru_2$	0.0023(5)	0.004(2)	0.0035(8)	0.003*
$Ni_{95}Ru_5$	0.0030(5)	0.005(2)	0.0043(9)	0.003*
	E_0 (eV)	S_0^2	ΔR (Å)	Δk (Å^{-1})
$Ni_{95}Mo_5$	0.5(9)	0.82(6)	1.2–5	3.9–12.6
$Ni_{99.8}Ru_{0.2}$	−2.8(9)	0.94(7)	1.2–5	2.6–13.9
$Ni_{98}Ru_2$	1.5(8)	0.88(6)	1.2–5	2.6–13.9
$Ni_{95}Ru_5$	1.2(7)	0.72(5)	1.2–5	2.6–13.9

The coordination numbers were fixed to the values of the pure compound.

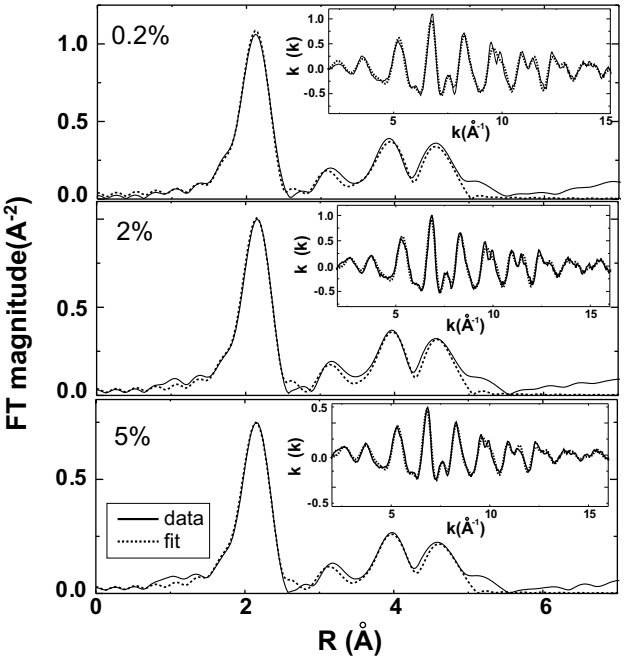

Fig. 3. Fourier-transforms of the EXAFS oscillations of the Ni:Ru samples (solid line) and fit (dotted line). The corresponding EXAFS spectra are given in the insets.

4.3. 5d elements Hf, Ta, W and Re in Ni

Fig. 4 depicts the Ni:Hf (0.2 and 5 at.%) Fourier-transformed k-weighted EXAFS spectra collected at the Hf K-absorption edge. The solid solubility of Hf in Ni is limited, and its maximum solubility below the eutectic temperature is estimated to be around 1.3 at.% [17]. In our earlier paper [18], we have performed comparative X-ray diffraction (XRD) and scanning electron microscopy (SEM) studies. Both XRD and SEM have revealed the presence of the $HfNi_5$ phase (fcc structure) in the $Ni_{95}Hf_5$ and $Ni_{98}Hf_2$ samples, whereas in the $Ni_{99.8}Hf_{0.2}$ sample the XRD and SEM provided an ambiguous picture, which was subsequently clarified by our preliminary EXAFS analysis. Here, the EXAFS analysis delivers enough quantitative information to identify two distinguishable configurations of Hf in Ni: (i) a majority of Hf atoms substituting for Ni in the $Ni_{99.8}Hf_{0.2}$ sample, and (ii) the majority of Hf atoms incorporated into the $HfNi_5$ phase within the $Ni_{95}Hf_5$ sample. Even at first sight while examining Fig. 4 it is evident that in the case of $Ni_{95}Hf_5$ (as compared to the $Ni_{98.2}Hf_{0.2}$ sample) we are dealing with a different local coordination: the position of the first peak is shifted toward greater distance, and instead of three distinct peaks corresponding to coordination shells of higher order we have a broad single second shell peak.

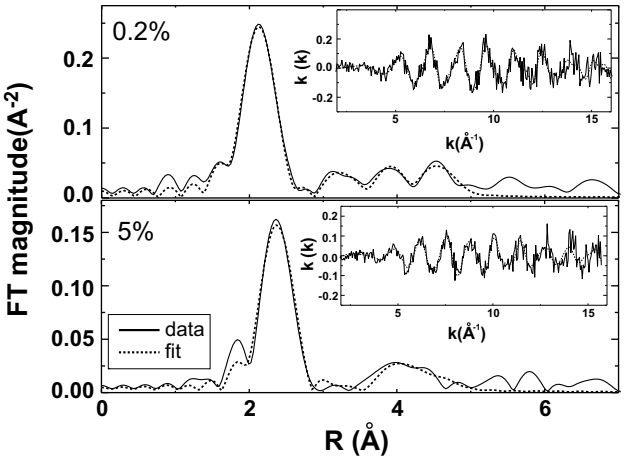

Fig. 4. Fit (dotted line) to the Ni:Hf data (solid line) using: (top) substitutional Hf in Ni model for 0.2 at.% Hf concentration, and (bottom) $HfNi_5$ model for 5 at.% Hf concentration. The corresponding EXAFS spectra are given in the insets.

The theoretical fitting standards for the $Ni_{95}Hf_5$ data were obtained using the F-43m space group of the pure $HfNi_5$ structure, with $a_0 = 6.683$ Å. For characterization purposes, the inclusion of the first four most dominant SS paths provided a satisfactory fit to the data. We notice an overall increase of the local bonds of approximately 1–2% as compared to the theoretical standards, which might be due to local distortions or clustering of this phase.

The $Ni_{99.8}Hf_{0.2}$ data was fitted using the pure Hf(Ni) substitutional standards, and the results of the fit are presented in Table 2. This model fits the data satisfactorily, the percentage misfit ($\mathscr{R}$-factor) being only 0.9%.

The Fourier-transforms of the $Ni_{98}Ta_2$ and $Ni_{95}W_5$ EXAFS spectra are given in Figs. 5 and 6, respectively. In the case of $Ni_{98}Ta_2$ the K-edge data is presented, whereas in the case of $Ni_{95}W_5$ only L_{III}-edge data were collected. The same substitutional situation, as described above, was used to fit the data up to the fifth coordination shell around the impurity. The misfits are somewhat larger when compared to the fits of the other systems, and we trace this back to the somewhat reduced statistics of the

Table 2
Fitted values from EXAFS data for the energy shift E_0, Debye–Waller factors σ, interatomic distances R, fit ranges ΔR and Δk, and S_0^2 for the first four coordination shells around Hf, Ta, W and Re

	R_1 (Å)	R_2 (Å)	R_3 (Å)	R_4 (Å)
$Ni_{99.8}Hf_{0.2}$	2.569(4)	3.58(1)	4.31(1)	5.0(2)
$Ni_{98}Ta_2$	2.541(6)	3.50(3)	4.34(1)	4.98(3)
$Ni_{95}W_5$	2.52(1)	3.51(4)	4.34(8)	4.6(2)
$Ni_{98}Re_2$	2.504(5)	3.54(1)	4.35(1)	5.0(1)
$Ni_{95}Re_5$	2.513(4)	3.55(1)	4.36(1)	5.0(1)
	σ_1 (Å^{-2})	σ_2 (Å^{-2})	σ_3 (Å^{-2})	σ_4 (Å^{-2})
$Ni_{99.8}Hf_{0.2}$	0.0020(4)	0.002(1)	0.003(1)	0.003*
$Ni_{98}Ta_2$	0.0014(6)	0.004(3)	0.001(1)	0.003*
$Ni_{95}W_5$	0.003(2)	0.006(5)	0.004(4)	0.002*
$Ni_{98}Re_2$(K)	0.0014(7)	0.001(2)	0.001(1)	0.00(4)
$Ni_{98}Re_2$(L)	0.0008(6)	0.001(1)	0.004(1)	0.00(9)
$Ni_{95}Re_5$(K)	0.0009(6)	0.002(2)	0.003(2)	0.00(3)
$Ni_{95}Re_5$(L)	0.0011(6)	0.001(2)	0.0022(9)	0.00(2)
	E_0 (eV)	S_0^2	ΔR (Å)	Δk (Å^{-1})
$Ni_{99.8}Hf_{0.2}$	−5(1)	0.85(6)	1.2–5	2.4–12.4
$Ni_{98}Ta_2$	−3(2)	1.1(1)	1.2–5	2.8–13.7
$Ni_{95}W_5$	5(3)	1.2(3)	1.2–5	4.2–11.0
$Ni_{98}Re_2$(K)	−8(1)	1.0(1)	1.2–5	4.0–14.2
$Ni_{98}Re_2$(L)	6(1)	0.84(8)	1.2–5	4.0–13.7
$Ni_{95}Re_5$(K)	−13(1)	0.8(1)	1.2–5	4.0–14.4
$Ni_{95}Re_5$(L)	6(1)	0.80(8)	1.2–5	4.0–13.7

The coordination numbers were fixed to the values of the pure compound.

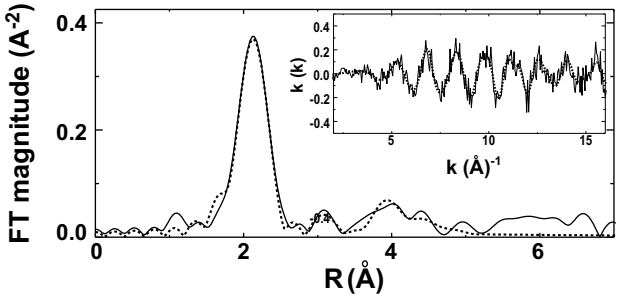

Fig. 5. Fit (dotted line) to the Ni:Ta data (solid line) for the sample with 2 at.% Ta. The k-weighted EXAFS spectra are given in the inset.

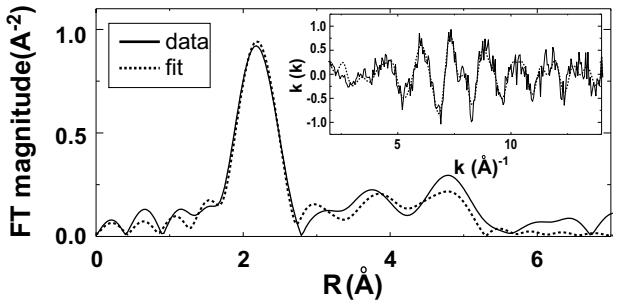

Fig. 6. Fit (dotted line) to the Ni:W data (solid line) for the 5 at.% W concentration. The corresponding k-weighted EXAFS spectra are given in the insets.

collected spectra. The $\mathscr{R}$-factors are up to 3% in both cases, indicating a somewhat larger but acceptable mismatch

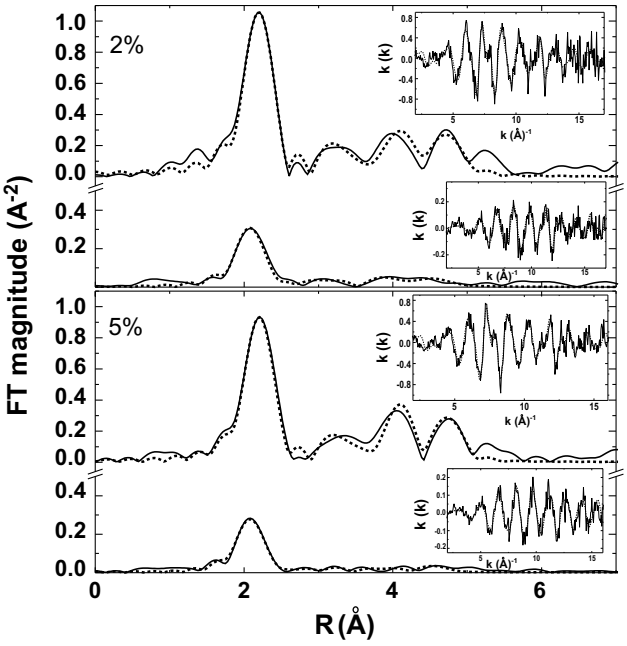

Fig. 7. Fit (dotted line) to the Ni:Re data (solid line) using: (top) substitutional Re in Ni model for the 2 at.%, and (bottom) for the 5 at.% Re concentration. The corresponding EXAFS spectra are given in the insets.

between fit and data, especially in the region between 3 and 5 Å.

In the case of Re-doped samples we were able to perform multiple data set fitting, owing to the fact that the EXAFS data were collected both around the Re K-edge and L-edge energies. Since the physical bond lengths are the same regardless from which absorption edge measurements we are extracting structural information, we were able to somewhat reduce the correlation between the fit parameters and obtain more accurate fits by fitting both absorption data sets simultaneously. Therefore, our fitting model accommodates the same ΔR parameters, but different E_0 and S_0^2 parameters in both data sets. As can be seen from Fig. 7, the obtained best fits to the $Ni_{95}Re_5$ and $Ni_{98}Re_2$ data are quite satisfactory, the goodness of fit being 2.6% and 2.8%, respectively. The values of the fitting parameters are given in Table 2. We decided to assign different σ^2 parameters for the corresponding paths in both data sets, which in principle could also have been regarded as mutual parameters, but at the end it is evident that within the error bars the values of σ^2 coincide.

5. Comparison with theory and discussion

From the results of the EXAFS analysis presented in the previous section we see that the most prominent lattice relaxation takes place in the first atomic shell around the impurity. The relaxation of this atomic shell, being our main focus in this work, is also determined with the highest accuracy, as compared to the more distant atomic shells. The structural information of the more distant shells is of

lesser accuracy and is mainly used to improve the fitting of the first shell. Our results undoubtedly support the conclusions that, except for the samples with higher Hf concentrations, all refractory elements under consideration substitute for Ni atoms at the Ni fcc lattice positions. Furthermore, all extracted NN distances are larger than the corresponding distance in pure Ni, and given the difference in metallic radii of Ni and the investigated 4d and 5d elements, they confirm the intuitive anticipations of outward relaxation around the impurities. There is a single point to be made, however, with regard to the next nearest neighbor (NNN) distance. The data in Tables 1 and 2 indicate that a sizable relaxation of the NNN distance is observed only in the case of Hf and Re, whereas for the others, the NNN distances are quite similar, within the error bars, to the corresponding values in the pure structure. Given that the contribution of this shell to the overall amplitude is small (coordination number 6) and that the error of the measured quantities reported in this work only includes the fitting errors (and not, for instance, the errors that might arise from the background procedure), no definite conclusion about the NNN relaxation around Mo, Ru, Ta and W can be made. It seems, however, that we indeed observe measurable lattice relaxation of the NNN shell where also the lattice relaxation of the NN shell is substantial (i.e. Hf and Ta).

Our calculated lattice relaxation corresponds to alloys with a concentration of ~3.7 at.% of impurity atoms when using the 27-atom supercell. The comparison with the experimental results is depicted in Fig. 8. For a general overview, we compare, wherever possible, the experimental distances for the samples with 2 or less at.%, (except for W in Ni with 5 at.%). In order to check the trends of the calculated distances with increasing supercell size, especially for Hf and Ta where we measured sizable relaxations, we also included the larger supercell results, that correspond to an impurity concentration of approximately 0.9 at.%. It is apparent that our calculations accurately reproduce the experimental trends, especially for a low concentration and a large supercell size.

The electronic structure provides further insight into the interplay between the bonding and lattice relaxation in these systems. In Fig. 9 (top) we present the total calculated spin density of states (DOS) of pure Ni, along with that of the NN Ni atoms to Hf in the 27-atom supercell. The DOS of the neighboring Ni atoms is practically undisturbed as compared to the pure Ni DOS, indicating that the interaction between the impurity and the host NN atoms is weak. This is found for all of the investigated impurities in Ni. This behaviour apparently leads to formation of virtual bound states (VBS) [19] localized on the impurity site and directly observed in the impurity d-DOS in the vicinity of the Fermi level or as empty VBS above the Fermi level, as depicted in Fig. 9 (bottom). Such VBS have been previously found for the 3d transition metal impurities in Ni [20], under the conditions that the valence difference between the host and impurity ΔZ, satisfies the relation $\Delta Z < -2$. Moreover, the energy position of the impurity d states seems to be correlated with the lattice relaxation in the vicinity of the impurity, as has been shown, for instance, for a range of 3d, 4d, and 5d impurities in

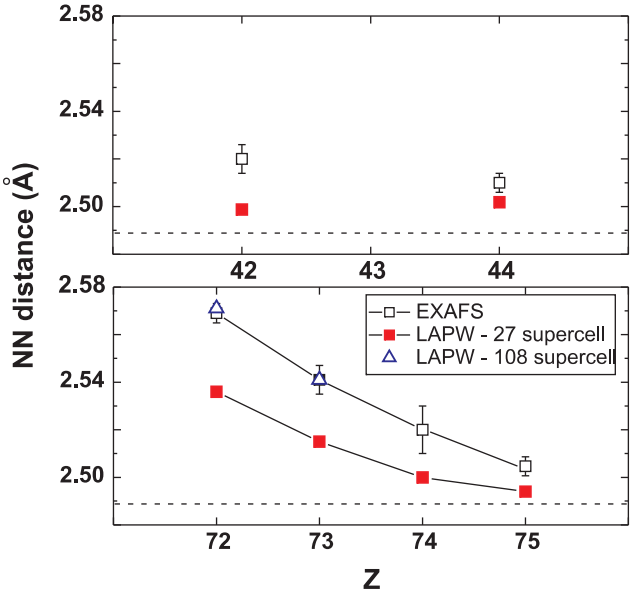

Fig. 8. Comparison between the experimentally extracted bond lengths (full squares) and the calculations. Open squares: 27-atom supercell; diamonds: 108-atom supercell, for the 4d (top) and 5d refractory elements (bottom). The horizontal dashed line denotes the NN distances in pure Ni.

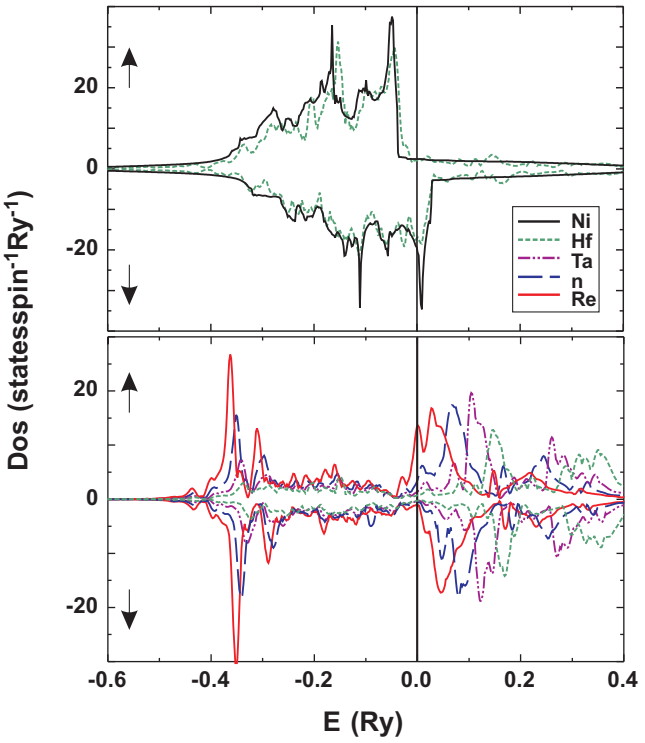

Fig. 9. Calculated total DOS at Ni in pure fcc Ni and at Ni around a NN Hf in Ni:Hf (top), and the partial d-DOS of Re, W, Ta and Hf (bottom).

Table 3
Bond lengths r_{NN}, magnetic moments μ, total charge of the majority spin d electrons n_d (up) and minority spin d electrons n_d (down) of the refractory elements in Ni as obtained by using a 27-atom supercell calculation

	r_{NN} (Å)	μ (μ_B)	n_d (up)	n_d (down)
Mo	2.499	−0.14	1.46	1.58
Ru	2.502	1.01	3.16	2.15
Hf	2.536	−0.10	0.59	0.68
Ta	2.515	−0.12	0.92	1.03
W	2.500	−0.13	1.35	1.46
Re	2.494	0.01	1.91	1.90

body-centred cubic (bcc) Fe [21] considering the connection between the position of the impurities d energy levels and their metallic radii.

Our calculations for Ta in Ni can be compared with the KKR calculations of Ref. [22], where a broader range of Ta concentrations has been investigated. In particular, the DOS are remarkably similar, and the agreement between the calculated Ta magnetic moments is also reasonable (−0.125 μ_B for 3.7 at.% Ta vs. −0.21 μ_B for 4 at.% [22]). As we go from Hf to Re, the calculated magnetic moments change from −0.10 μ_B for Hf, via −0.12 μ_B for Ta and −0.13 μ_B for W to a practically negligible value of 0.01 μ_B for Re. The reason for the negative values of the magnetic moments at Hf, Ta and W is the smaller separation between their spin down bands and those of Ni, which through interaction fills this channel slightly more than the majority spin channel. Only in the case of Re is the direction of the magnetic moment reversed, when the process of filling the higher lying d-bands already starts.

A summary of the calculated bond lengths, magnetic moments and partial charges is given in Table 3. Since the MT spheres were set to be equal for all of the 5d elements, the total integrated d charge (within the MT spheres) can be an indication of the trends in the charge transfer. We see that the refractory elements' d electrons are being increasingly delocalized as we go from Hf (where 0.72 e is leaking) to Re (1.19 e), which obviously stabilizes the structure leading to stronger bonds and less pronounced lattice relaxation.

6. Conclusions

In conclusion we have measured the local bond lengths around Mo, Ru, Hf, Ta, W and Re in Ni. We have found systematic outward relaxation in the range from ∼0.6% for Ru up to ∼3.2% for Hf as compared to the distances in the pure host. The ab initio calculations with the supercell LAPW method appear to be able to reproduce the experimental tendency of lattice relaxation, especially when the supercell impurity concentration closely matches the experimental one. This gives confidence that ab initio methods could predict the local structure with satisfactory accuracy even when the experimental verification is not feasible. Clearly, from the standpoint of applications for superalloy design, these results should be complemented by additional experimental and theoretical input on the γ' phase – a study which is currently under way.

Acknowledgement

The authors are grateful to the HASYLAB staff at DESY, in particular to J. Wienold and E. Welter. We very much appreciate P. Szimkowiak's help in sample preparation. V.K., J.B.-C. and B.C. would like to acknowledge the support from the Serbian Ministry of Science under the Grant No. 141022G.

References

[1] Giamei AF, Auto DL. Metall Trans A 1985;16:1997.
[2] Rüsing J, Wanderka N, Czybayko U, Naundorf V, Mukherji D, Rösler J. Scripta Mater 2002;46:235.
[3] Wang SY, Wang CY, Sun JH, Duan WH, Chao DL. Phys Rev B 2001;65:35101.
[4] Chen K, Chao LR, Tse JS. J Mater Sci Lett 2003;22:603.
[5] Bruno G, Schumacher G, Pinto HC, Schulze C. Metall Mater Trans A 2003;34A:193.
[6] Völkl R, Glatzel U, Feller-Kniepmeier M. Acta Mater 1998;12:4395.
[7] Pineau A. Acta Mater 1976;24:559.
[8] Prem M, Krexner G, Pettinari-Sturmel F, Clement N. Appl Phys A 2002;74:1112.
[9] Pettinari F, Prem M, Krexner G, Caron P, Coujou A, Kirchner HOK, et al. Acta Mater 2001;49:2549.
[10] Ravel B, Newville M. J Synchrotron Rad 2005;12:5375.
[11] Ankudinov AL, Ravel B, Rehr JJ, Conradson SD. Phys Rev B 1998;58:7565.
[12] Blaha P, Schwarz K, Luitz J. Comput Phys Commun 1990;59:399.
[13] Blaha P, Schwarz K, Madsen GKH, Kvasnicka D, Luitz J. WIEN2K, an augmented plane wave + local orbitals program for calculating crystal properties. Karlheinz Schwarz, Technische Universitat Wien, Austria; 2002.
[14] Perdew JP, Burke S, Ernzerhof M. Phys Rev Lett 1996;77:3865.
[15] Li GG, Bridges F, Booth CH. Phys Rev B 1995;52:6332.
[16] Scheuer U, Lengeler B. Phys Rev B 1991;44:9883.
[17] Hajjaji M. J Alloys Compd 1998;274:185.
[18] Umicević A, Mahnke H-E, Cekić B, Grbović J, Koteski V, Belošević-Čavor J. Mater Sci Forum 2006;518:325.
[19] Anderson PW. Phys Rev 1961;124:41.
[20] Mertig I. Rep Prog Phys 1999;62:237.
[21] Morinaga M, Yukava N, Adachi H. J Phys F: Met Phys 1985;15:1071.
[22] Moghadam NY, Stocks GM. Phys Rev B 2005;71:134421.